This is a peer-reviewed, accepted author manuscript of the following article: Thomason, J. L., & Rudeiros Fernández, J. L. (2021). Modelling the influence of fibre internal structure on the measured modulus of technical natural fibres. *Composites Part A: Applied Science and Manufacturing*, [106478].
https://doi.org/10.1016/j.compositesa.2021.106478

Modelling the influence of fibre internal structure on the measured modulus of technical natural fibres

James L. Thomason* and Jose L. Rudeiros-Fernández

University of Strathclyde, Department of Mechanical and Aerospace Engineering, 75 Montrose Street, Glasgow G1 1XJ, United Kingdom.

*Corresponding Author, james.thomason@strath.ac.uk Tel:0044-141-5482691

Abstract

The internal structure, cross section area (CSA) and mechanical properties of palm and coir fibres were investigated using SEM on cryotome cut samples, tensile measurements of single technical fibres at three gauge lengths and optical microscopy of fibre cross sections. The measured technical fibre modulus was significantly dependent on gauge length and CSA. Two theoretical approaches were developed to fit the observed modulus dependence on fibre CSA. These calculated the measured technical fibre modulus as a function of the dimensions of the technical and elementary fibres combined with modulus of the elementary fibres and the efficiency of the inter-level interface to transfer stress across consecutive levels within the fibre. Palm fibre results gave good correlation between experimental observations and theoretical predictions. The modulus dependence of coir fibres on CSA was less well defined due to a higher level of property variability which led to poorer correlations with fitting model values.

Keywords: A Natural fibres, B Microstructure, B Mechanical properties, B Stress transfer, C Analytical modelling

1. Introduction

Natural fibres derived from plants are lignocellulosic structures, normally found as elementary fibres (individual plant cells) assembled together into bundles which are generally produced in the stem of the plant or as part of the leaves but also in fruit, seed, roots, grass and wood [1,2]. For the purposes of clarity, in this paper, the term natural fibre or technical fibre is used to denote an assembly of elementary fibres. The mechanical properties of natural fibres is influenced by many variables such as their chemical composition, structure, age, growth climate conditions, harvest and retting process [3-6]. Mechanical properties can vary greatly depending on the type of natural fibre. Furthermore, mechanical properties also vary within the same type of plant. Despite this high level of variability, which can only be viewed as a major drawback in terms of their processability and performance, many authors suggest that natural fibres have a promising future for use as a realistic composite reinforcement in high throughput, high performance applications. Much of this enthusiasm is predicated on a few examples of natural fibres which have a relatively high axial stiffness. Maintaining this enthusiasm requires the ignoring of the very low transverse and shear modulus natural fibres [7-12]. When examining the modulus of natural fibres it is interesting to note that, whereas manmade fibres offer a product where the stiffness of each fibre is normally close to the expected datasheet value, the stiffness of individual natural fibre varies greatly from fibre to fibre. It has been also noted by a number of authors that there appears to be a relationship between natural fibre modulus and its cross sectional area [13-20].

It is worthwhile also noting at this point that when characterising natural fibre mechanical properties, it is important to take into consideration the non-circular nature of their cross sectional area (CSA) [13]. Considering natural fibres to have a circular CSA and calculating fibre properties based on diameter measurements from transverse observations can lead to significant errors. It has also been reported that fibre diameter has a further indirect effect on the mechanical properties and a Young's modulus dependence on CSA has been reported for natural fibres [14-17]. Baley [14] showed how flax Young's modulus decreased for increasing fibre diameter, suggesting that not deducting the lumen from the gross measured CSA, non-constant CSA along the fibre length, presence of defects and variability in fibre's composition could cause the observed correlation. Other authors [18-20], attempted to use an empirical expression, based on the Griffith model [21], to interpolate the results.

In this paper we present the results of a study of the modulus of single fibres of coir and date palm leaf and how the modulus value varies with CSA. We further present the development of two theoretical models which can assist in the explanation of the observed Young's modulus dependence on fibre CSA.

2. Experimental

2.1. Observation of fibre internal structure

The date palm leaf and coir (coconut fruit husk) fibres were both provided by SABIC. Individual natural fibres were embedded vertically in a plastic mini-mould that was filled with optimal cutting temperature (OCT) embedding matrix (normally used for embedding tissue samples). The samples were then placed in a freezer where the embedding matrix solidified, after which they were sectioned into 16 μm slices using a cryotome. The slices were gold coated for observation using a HITACHI SU-6600 scanning electron microscope.

2.2. Tensile testing of single technical fibres

Tensile testing of single technical fibres was carried out following the main recommendation on standards ASTM D3822 and ASTM C1557. Palm and coir fibres were individually separated until no fraying could be seen with the naked eye. Thereafter, fibres were mounted on paper card frames made from 250 g/m^2 card, where a window with the desired gauge length had been previously cut out. Initially fixed to the card frames by double-sided tape, fibres were subsequently fixed by Loctite Gel Superglue. The fibre cross section area (A_{cf}) was first estimated by assuming a circular cross section. All mounted fibres were photographed at the middle point of the gauge length under transverse observation using a Leica microscope at 10x magnification. Three "diameters" in each picture were measured using the software ImageJ as illustrated in Figure 1. For this initial stage, fibre diameter (D_f) was estimated as the average of these three measurements. Fibre strength and Young's modulus was characterised by tensile testing, using an Instron 3342 tensile testing machine with a 100 N load cell. The cross-head displacement rate was set at 5% strain per minute. For the tensile test, card and fibre were clamped up to the gauge length in order to avoid any slippage. For each fibre test the sides of the card frame were carefully cut with scissors and then the load as a function of cross-head displacement was recorded and subsequently used to calculate the fibre strength and Young's modulus. Three gauge lengths (5, 10 and 20 mm) were used for each fibre in order to correct the fibre modulus for compliance effects. True fibre modulus E_f is related to the measured modulus E by

$$\frac{1}{E} = \frac{1}{E_f} + C_s \frac{A_f}{L_0} \quad (1)$$

where E is the modulus measured at gauge length L_0 and C_s is the system compliance.

2.3. Cross section area and perimeter measurement

The true CSA (A_f) and perimeter (P_f) of natural fibres were characterised in order to improve the estimation of the mechanical properties of the fibres. The differences between A_f and A_{cf} due to the typical non-circular cross section of most natural fibres has been well documented [13,22]. The process of measurement of the true fibre CSA is illustrated in Figure 2. After tensile testing, the bottom and top ends of the tested fibre samples were removed and fixed to 250 g/m^2 card in vertical position. These cards with the fibres were then inserted into a mould that was subsequently filled with resin. Once set, the resin blocks were then ground and polished enabling the fibre cross sections to be photographed using an Olympus GX51 microscope. For every picture, the cross-section was traced and exported for analysis of A_f using ImageJ software. Higher magnification photographs of the CSAs were also used to characterise the internal structure of palm and coir fibres in terms of CSA and aspect ratio of elementary fibres (see Figure 3).

3. Results and discussion

3.1. Natural fibre internal structure

SEM images of the complex internal structure of coir and palm fibres are shown in Figure 4. It can clearly be observed how both fibre types are made up by the addition of many elementary fibres or cells joined together. These cells are cemented together by the middle lamella, which is generally a pectin-rich and/or lignin-rich layer [2]. In the case of both fibres, the shape and size of elementary fibres and thickness of the cell's wall varied greatly through the CSA. The overall CSA (which in most of the cases differed from a circular estimate of CSA) also varied in shape and size depending on the fibre. These variations can lead to high levels of anisotropy, non-symmetrical stress distributions within the fibre and high variability of fibre properties. Furthermore, failures running across the internal interface between elementary fibres could often be observed (arrowed in the upper two micrographs of Figure 4). These kind of debonded interfaces could be due to sample preparation, where fibres undergo shear stresses while being cut in the cryotome. In any case, these internal failures (including debonded intra-fibre interfaces and elementary fibre micro-cracks) could lead to sudden mechanical failure or a decrease of the fibre's mechanical

properties, as has been suggested for other natural fibres [23,24]. Additionally, when these fibres are embedded into a composite matrix system, internal failures could rapidly propagate from the fibre to the fibre-matrix interface and subsequently to the matrix. If the composite fibre-matrix interfacial shear strength (IFSS) is higher than the inter-elementary fibre IFSS, then failure initiation will take place within the fibre [25,26]. Closer inspection of the elementary fibres in Figure 4 revealed further non-uniformity of cellular walls. In some cases, considerable separation could be observed between the different parts of the cell wall, (arrowed in the lower two micrographs in Figure 4) giving the appearance that the primary and secondary walls may not be well bonded. As previously discussed, this could ultimately lead to sudden mechanical failure under load, reduction of fibre properties or non-uniform stress distributions within the fibre.

3.2 Geometry of fibres

Optical microscopy of fibre in the transverse directions showed that the CSA of coir and palm fibre varied significantly. The range of observed "diameters" for palm fibres varied from approximately 100 to 1000 μm. In the case of coir fibres, the range was slightly smaller, where fibre "diameters" varied from approximately 100 to 500 μm. Direct observation by optical microscopy of the cross sections of post-tested fibres confirmed the large CSA range (especially for palm fibre). Figures 5 and 6 compare the CSA based on "diameter", assuming a circular CSA, and CSA based on direct observation. As Thomason *et al* [13] pointed out, the CSA based on the "diameter" method is a less accurate procedure and normally leads to underestimation of the true fibre mechanical properties by overestimating the fibre CSA. In this case, from the slope of the least squares fitted straight line, it can be asserted that an overestimation of the CSA could be approximately 20 % for palm fibres and 40 % for coir fibres. This relative difference between true and estimated CSA is significant although not as high as some other natural fibres, such as sisal or flax, where overestimations of 100-150 % have been documented [13].

Figure 7 illustrates the CSA distribution of palm and coir elementary fibres. A total of 420 elementary fibres were measured for this analysis. The distribution of the average CSA of coir elementary fibres was somewhat narrower than that of the palm elementary fibres. This resulted in a higher average value of palm elementary fibre CSA of 130 μm^2 compared to 103 μm^2 for coir elementary fibres. A two-sample *t*-test of the average values showed this to be a significant difference even at 99% confidence level. The true CSA distributions of the fibres which were tensile tested are illustrated in Figure 8. For palm, most of the fibres were within the range between 0.01 and 0.3 mm^2. In the case of coir, the range is significantly smaller, with

most of the fibres within the range between 0.01 and 0.08 mm^2. The average values for the palm and coir elementary CSA and technical fibre CSA are summarised in Table 1.

3.3 Tensile properties

Typical stress-strain curves for coir and palm fibre are shown in Figure 9. Two distinct regions can be observed for both fibres. There is an initial elastic deformation region, up to about 2% strain, above which there is a longer plastic deformation region. Coir and palm are both fibres with high cellulose microfibril angle (MFA) [3,27-29]. Such fibres normally exhibit bi-phasic stress-strain behaviour, which is related to the variation of MFA during deformation [27,30,31] and the interaction between cellulose microfibrils and the rest of the cellular wall matrix components [32]. At the yield point, the shear stress of the matrix components of the cellular walls is exceeded and cellulose microfibrils start sliding [32]. It has been reported that coir fibres can partially recover their properties even after such plastic deformation [27].

The average values obtained for Young's modulus, tensile strength and failure strain are summarised in Table 2 and are generally in line with other published values [5,6]. The fibre modulus and strength were calculated using individual fibre CSA obtained by both the "diameter" method and the direct observation method as discussed above. It was found that the "diameter" method did underestimate the mechanical property values by up to 15%. The values of Young's modulus calculated using the true CSA for coir and palm are illustrated in Figure 10. All results are illustrated with error bars representing 95% confidence limits. It can be seen that the measured fibre modulus increases with increasing gauge length as predicted by Equation 1. Regarding the strength values for palm fibre, the average decreased with increasing gauge length. However, two-sample *t*-tests of the average strength at the three different gauge lengths revealed no significant differences at 95% confidence level. Therefore, for palm, since there was no significant difference in fibre strength, taking an overall average is valid. In the case of coir fibre, two-sample *t*-tests of the average CSA corrected strength at the three different gauge lengths showed significant differences between 5 - 10 mm and 10 - 20 mm at 95% confidence levels. However, no significant difference was found between 5 and 20 mm. These differences could indicate that the CSA distribution, which was approximately 50% higher for the 10 mm gauge length samples, along with natural fibre variability may have had an effect on the average tensile strength results. A two-sample *t*-test of the overall CSA corrected average strength of palm (116 MPa) and coir (149 MPa) showed a significant difference in the averages at the 95% confidence level. From Table 2, it can also be noted that the failure strain for both fibres decreased with

increasing gauge length. However, in the case of palm two-sample *t*-tests of the average failure strain showed no significant differences at 95% confidence level between 10 mm and 20 mm sets (*p*-value = 0.134). Nevertheless, for the coir fibres two-sample *t*-tests of the average failure strain showed significant differences at 95% confidence level between 5, 10 and 20 mm sets. As in the case of fibre strength, natural fibre variability and differences in the diameter distribution of sets may have had certain influence.

Regarding the analysis of Young's modulus, in the case of both fibres, there was a clear gauge length effect. It is well known that the values obtained during single fibre testing can be affected by the gauge length of the fibre [13]. Most manmade fibres have a very much smaller CSA distribution and the compliance corrected fibre modulus is often obtained using Equation 1 with the average modulus values at each gauge length and Af set to a constant. Using that approach the compliance corrected values obtained for palm fibre was 3.8 GPa and for coir fibre 4.0 GPa both within the normal range of value reported for these two types of fibre. In Figure 11 the modulus dataset for all gauge lengths is plotted according to Equation 1 and a straight line fitted to the data using the least squares method. Using the value of y-axis intercept the compliance corrected Young's modulus (E_f) obtained for palm fibre was 2.5 GPa and for coir fibre 2.9 GPa. In both cases this compliance corrected (according to Equation 1) value of fibre modulus appears to be lower than the average value obtained at 20 mm gauge length for each respective fibre and significantly lower than the values obtained above for compliance correction of the average modulus values. This is a most unexpected result.

Using the CSA dependent version of Equation 1 with fixed gauge length and plotting the datasets for each measured gauge length resulted in a set of modulus versus gauge length values very similar to those shown in Table 2. However, as shown in Table 3, this exercise indicates that the value for the compliance of the system (C_s in Equation 1) is not a constant but appears to be inversely dependent on test gauge length. This behaviour has also been observed by Defoirdt *et al* in a study of the tensile properties of a number of natural fibres and they attributed the effect to slippage in the clamps [33]. However, they also concluded that these effects are small in case of coir, where plastic deformation probably starts before significant slip and test-set-up compliance can influence the results. Moreover, the suggestion of slippage as a cause of extra contribution to the crosshead position estimate of strain is based on a single reference of Joffe *et al* [34] which is not based on single fibre testing but fragmentation of a single fibre in a block of resin where the applied forces are orders of magnitude higher. Indeed in Joffe's paper slippage is only mentioned once

as a possible source of error without any further evidence being presented. Given the random nature of slippage it seems likely that, if occurs at all, it would not occur continuously during a tensile test but would be evidenced by one, or more, drops in load in the load -displacement curve. There was no sign of such a phenomenon in the load-displacement curves of the fibres tested in this work. In fact, a simple exploration of the role of the various factors in Equation 1 revealed that another explanation for the above observations on measured fibre modulus could be if the actual fibre modulus (E_f) had an inverse dependence on the CSA of the fibre.

3.4. Young's modulus dependence on cross-section area

The data for fibre modulus have been replotted in Figure 12 as a function of gauge length and CSA, where the data sets have been divided into three CSA groups (thin, medium, thick) of sizes appropriate for each fibre type. The data in Figure 12 clearly show that the dependence of measured fibre modulus on gauge length increases as fibres become thicker. The three modulus values for the different thickness ranges were all significant at the 95% confidence level for the 5 mm gauge length measurements, whereas for 20 mm gauge length the differences in average modulus values for the different thickness ranges was not significant, with differences at 10 mm gauge length showing intermediate levels of significance. When analysing the effect of fibre CSA (A_f) on the Young's modulus of flax fibre Baley [14] suggested that this could be a result of factors such as, non-constant CSA along the fibre length, ignoring the lumen when calculating the CSA, and the presence of defects and variability in the composition along the fibre length. However, there is another possible explanation for this behaviour. Natural fibres are made up of single elementary fibres or cells, joined together by the middle lamella which is mainly composed of pectin and lignin. While analysing the internal structure of natural fibres, several signs of damaged or weak inter-elementary fibre interface were observed. When analysing the micro-mechanical behaviour of fibres, shear-lag theories assume no or little stress transfer through fibre's ends. Consequently, most of the applied stress, whether in a fibre tensile test or in a loaded composite, is transferred through fibre's external surface, known as fibre-matrix interface. A lack of efficiency in transferring stress inside the fibre and on to the individual elementary fibres across the CSA would result in a CSA dependency of the Young's modulus.

If the middle lamella is not able to efficiently transfer stress from the outer to the inner elementary-fibres, this would lead to the elementary fibres located in the perimeter of the CSA supporting considerably

higher levels of stress compared to those in the interior of the fibre. Similar effects due to the lack of stress transfer across internal structures have been reported in studies of the modulus of multi-walled carbon nanotubes (MWCNT) [35,36]. The shear-lag nature of the problem, i.e. the longer the stress transfer length the greater the probability that all elementary fibres will approach carrying their full share of the applied load, also leads to the prediction that this effect would be less evident for higher gauge lengths, as observed in Figure 12. For this reason, the treatment of experimental data was focused on the Young's modulus of fibres tested at 5 mm gauge length. In the case of palm, the trend appeared to be clearer, perhaps, due to a higher range of CSA included in the study in comparison with coir.

3.5 Honeycomb and circular models

In this section, a mathematical model of the structure of natural fibres is developed in order to analyse the effects of stress transfer on the observable Young's modulus. Palm and coir fibres are modelled as cellular solids built up of hexagonal cells. This approach has been previously used to analyse a broad range of natural materials [37-40] such as wood, cork and bone. A fibre is considered to be made up of equally sized, perfectly hexagonal cross section elementary-fibres or cells arranged together to form a honeycomb structure. Every element of the structure is assumed to have the same isotropic mechanical properties. In the honeycomb model, the elements are assumed to be continuous in the longitudinal direction, and have the same length as the natural fibre structure.

The basic hexagon cell is defined as having a side length l and a cross section area $A_c = 2.6l^2$. The structure builds up around a central cell at the centre of the fibre as illustrated in Figure 13. The variable n is an integer defined as the number of *levels* of the structure, where the central cell is considered as the first level (i.e. $n = 1$). It is assumed that all the elements in the same n-level are under the same homogenous stress when the fibre is loaded externally. Normal stresses and Poisson's ratio effects are neglected in the model. The number of cells in the n-level, n_{pc} is given by

$$n_{pc} = 6(n-1);\ n > 1 \tag{2}$$

Consequently, the area of the n-level is defined,

$$A_n = 9\sqrt{3}(n-1)l^2;\ n > 1 \tag{3}$$

The external perimeter of the n-level P_n is defined in (1.14).

$$P_n = 6(2n-1)l;\ n > 1 \tag{4}$$

The total number of cells n_{tc} in a fibre made up of n-levels is given by

$$n_{tc} = 1 + 6\sum_{i=2}^{n}(i-1)\ ;\ n > 1 \tag{5}$$

For each n-level, a circumference can be defined where the cells can be inscribed as shown in Figure 13. The radius of the circumscribed (r_{cc}) and inscribed (r_{ci}) circumference is given by Equations 6 and 7.

$$r_{cc} = \frac{l}{2}[1 + 3(2n-1)^2]^{\frac{1}{2}} \tag{6}$$

$$r_{ci} = \frac{\sqrt{3}}{2}l(2n-1) \tag{7}$$

Therefore, a fibre with a CSA A_f, for a defined l would have an equivalent fibre of n-levels, approximating $A_f \sim \pi {r_{cc}}^2$ or $A_f \sim \pi {r_{ci}}^2$. For a defined value of l, the value of n would then be approximated as the nearest integer to the number provided by either Equation 8 or 9..

$$n = \frac{1}{2}\left(1 + \frac{1}{\sqrt{3}}\sqrt{\left(\frac{4A_f}{\pi l^2} - 1\right)}\right) \tag{81}$$

$$n = \frac{1}{2}\left(1 + \frac{2}{l\sqrt{3}}\sqrt{\frac{A_f}{\pi}}\right) \tag{9}$$

As the first consideration, if there is no stress transfer between the cells in the perimeter and the internal cells, fibres would be equivalent to hollow fibres as illustrated in Figure 14. In the case of such hollow fibres, equivalent to no internal interfacial stress transfer conditions, the effective CSA is A_n and the true Young's modulus E_{fr} is related to the measured fibre modulus E_f by

$$E_f = \frac{A_n}{A_T}E_{fr} \tag{10}$$

where A_T is the area of the total number of cells in all n levels. This can be re-written as

$$E_f = \frac{A_n}{A_T}E_{fr} = \frac{n_{pc}A_c}{n_{tc}A_c}E_{fr} = \frac{6(n-1)}{1 + 6\sum_{i=2}^{n}(i-1)}E_{fr} \tag{11}$$

where Ac is the area of a single cell and n is calculated according to Equation 8 or 9.

Shear stress transfer between the n levels can now be can be implemented in a similar manner to that used in the modelling of MWCNT [36]. In Figure 15, the honeycomb fibre structure, with a cross section illustrated in Figure 13 is represented by the plane yz perpendicular to x, running along the fibre's longitudinal axis. The interactions between the different levels of a fibre with n-levels are illustrated in Figure 16. The shear stress transfer is expressed through a series of τ_i which are defined as apparent

interfacial shear stress along the inter-level interfaces. The efficiency of interfacial stress transfer is defined as η, where $0 \leq \eta < 1$ (i.e. $\eta = 0$ represents a situation where no stress is transferred through the interface). The stress applied to the fibre σ_0 is directly transferred to the outer level. For a fibre of length L and when $\eta = 1$ (i.e. perfect stress transfer), the extension ΔL_n of the outer level (i.e. level n) is

$$\Delta L_n = \frac{\sigma_0 L}{2E_{fr}} - \frac{P_{n-1}L^2}{4A_n E_{fr}}\tau_n \tag{12}$$

The extension of any intermediate level ΔL_i is defined in terms of the interfacial stresses as

$$\Delta L_i = \frac{P_i L^2}{4A_i E_{fr}}\tau_{i+1} - \frac{P_{i-1}L^2}{4A_i E_{fr}}\tau_i \tag{13}$$

At the central level (i.e. level 1), the extension is defined as

$$\Delta L_1 = \frac{P_i L^2}{4A_1 E_{fr}}\tau_2 \tag{14}$$

For the case analysed here where $\eta = 1$, the extension of all levels is identical. Consequently the apparent interfacial shear stress τ_i must be given by

$$\tau_i = \frac{2\sigma_0 A_n}{P_{i-1}L}\left(1 - \frac{\sum_{j=i}^{n} A_j}{A_T}\right) \tag{15}$$

Once the variation of τ_i is obtained, by substituting Equation 15 into Equation 12 and adding the η parameter, the extension of the external level can be re-written as

$$\Delta L_n = \frac{\sigma_0 L}{2E_{fr}}\left(1 - \eta\left(1 - \frac{A_n}{A_T}\right)\right) \tag{16}$$

The measured Young's modulus of the fibres E_f is

$$E_f = \frac{\sigma}{\varepsilon} = \frac{\sigma_0 A_n}{A_T}\frac{L}{2\Delta L_n} \tag{17}$$

Combining Equations 16 and 17 gives relationship between the measured Young's modulus of the fibres E_f and the true fibre modulus E_{fr}

$$E_f = \frac{A_n}{A_T}\left(1 - \eta\left(1 - \frac{A_n}{A_T}\right)\right)^{-1} E_{fr} \tag{18}$$

Substituting for A_n and A_T, the measured Young's modulus of the fibres E_f for $n > 1$ is defined as

$$E_f = \frac{6(n-1)}{1 + 6\sum_{i=2}^{n}(i-1)}\left(1 - \eta\left(1 - \frac{6(n-1)}{1 + 6\sum_{i=2}^{n}(i-1)}\right)\right)^{-1} E_{fr} \tag{19}$$

For the no stress transfer case where $\eta = 0$, this is equivalent to Equation 11 and for a full stress transfer scenario where $\eta = 1$, then $E_f = E_{fr}$. Figure 17 maps the resulting values ratio E_f / E_{fr} for a range of n and η values.

It is also possible to define a circular structure model which can be compared to the honeycomb model. This model is defined as illustrated in Figure 18. In this case, elementary fibres are assumed to join together in a series of homogenous levels. As in the honeycomb model, it is assumed that the stress is uniform within the same n-level. Normal stresses and Poisson's ratio effects were again neglected. Based on the definition given in Figure 18a, the external radius of each level will be determined according to

$$r_n = r_c(2n - 1) \tag{20}$$

where the value of $2r_c$ could be taken as the diameter of a single elementary fibre. Consequently, the area of each level is given by

$$A_n = 8\pi {r_c}^2 (n - 1) \tag{21}$$

The number of levels in a fibre with a CSA of A_f can be calculated using

$$n = \frac{1}{2}\left(1 + \frac{1}{r_c}\sqrt{\frac{A_f}{\pi}}\right) \tag{22}$$

Similarly to the honeycomb model, the value of n is approximated as the nearest integer to the number obtained. Equation 19 can then be re-written as

$$E_f = \frac{8(n-1)}{(2n-1)^2}\left(1 - \eta\left(1 - \frac{8(n-1)}{(2n-1)^2}\right)\right)^{-1} E_{fr} \tag{23}$$

The results of both the honeycomb and circular models are compared in Figure 19 where it can be clearly seen that the predictions of the two models are approximately equivalent, with overlapping curves for the E_f/E_{fr} ratio versus n. Since both models are formulated for using n and η, this allows inclusion of a cell size dependence on CSA. It is interesting to note in Figure 19 (and also 17) that only a small reduction in the interfacial stress transfer parameter from 1.0 to 0.9 can produce a drop in the measured modulus of larger natural fibres by more than 50%. This highlights the need to reduce the effective diameter of natural fibres to be used as a composite reinforcement to as close as possible to the elemental fibre value in order to maximise their reinforcement potential. Conversely this also illustrates the challenge of using low cost (thick) technical fibres in terms of achieving adequate composite performance. Furthermore, these results only point out the issue of weak internal interfaces in natural fibres on the stiffness of the fibre. However,

such weak internal interfaces are very likely to fail under low applied load (as in Figure 4) which will lead to initiation sites for composite failure, thus lowering strength and impact performance [8,9,25,26,41].

3.6 Experimental data and theoretical predictions

It should be stressed here that in any attempt to fit these theoretical models to experimental observations it is important to be aware of the limitations of the model with regard to the significant simplification of the variability of natural fibres properties. Moreover, due to the previously discussed effect of fibre length in relation to the shear-lag and compliance effects (which these models do not take into consideration), the theoretically calculated E_{fr} is restricted to the gauge length of the experimental observations.

The main parameters of the honeycomb and circular models are the cell size l ($l \sim r_c$), the Young's modulus of elementary fibres E_{fr} and the internal interfacial stress transfer efficiency η. In an attempt to probe how the inter-fibre variability of these parameters affect the predicted value of E_f versus the fibre CSA (A_T), a random set of parameters was generated. A set of 30 data points $[E_f, A_T]_R$ was generated based on the CSAs of the coir 5 mm gauge length set and randomly distributed parameters η between 0.5-0.8, l between 5-7 μm and E_{fr} between 2-5 GPa, using Equations 8 and 19. Furthermore, another set of 30 data points were generated based on the same CSAs but using the average values $\bar{\eta}$ (0.63), $\bar{l}$ (5.98 μm) and $\overline{E_{fr}}$ (3.51 GPa) of the previous randomly distributed parameters. Results for the prediction of E_f versus CSA are illustrated in Figure 20. It can be clearly seen that a low variability of these three parameters will dramatically affect the distribution of E_f versus A_T. It is clear from these results that, if there is high inter-fibre variability of properties, it will be a difficult task to estimate η, l, and E_{fr} from experimental observations, especially if only a limited range of CSA is available. It should also be noted that if a Young's modulus dependence on CSA is observed, the validity of the normal compliance correction is questionable. The correction based on Equation 1 assumes a value of E_f that is not dependent on CSA. Therefore, individual corrections of Young's modulus were not considered and as an initial approximation, only CSA corrected values were used. For the treatment of the experimental data, cell size parameters l and r_c, with $l \sim r_c$, were considered constant over the full CSA range. The value of l was calculated as the average of the single l-values generated from each measured CSA of elementary fibre, according to $A_c = 2.6l^2$ (as in Figure 13). The average l was 6.9 μm for palm and 6.2 μm for coir respectively. A two-sample *t*-test of the average values showed a significant difference at 99% confidence level.

The models, based on Equations 19 and 23 which include η and E_{fr} as fitting parameters, give the observable E_f as a function of the fibre CSA A_T, for certain given cell size l. The models were fitted to the experimental data using the standard least-squares method. Modulus versus CSA from experiment and the hexagonal cell model is shown in Figure 21 for palm fibres. (As expected from Figure 19 the circular model produced almost identical results and is therefore not shown). The calculated values for (η, E_{fr}) based on honeycomb and circular models are summarised in Table 4. The R^2 values indicate a good correlation between the models and experimental data. In the case of results for coir fibre shown in Figure 22 a much larger scatter is observed in the experimental data, although the calculated model values do generally pass through the experimental data. As predicted from the sensitivity analysis shown in Figure 20, these results may indicate a possible higher inter-fibre variability of properties in coir fibre. Certainly the R^2 value of the model fitting results for coir in Table 4 is low and not much significance can be placed on the estimated coir elementary fibre modulus. In contrast the fit for the palm fibre is much better and the high value of R^2 gives much higher confidence in the estimated value for the palm elementary fibre modulus."

4. Conclusions

The complex internal structure of coir and palm technical fibres revealed high variability in terms of the shape and size of the elementary fibres and their cell wall thickness. These variations along with non-circular and variable overall CSA and internal voids could ultimately lead to high levels of anisotropy, non-symmetrical stress distributions within the fibre and high variability of the technical fibre properties. Moreover, weak inter-elementary fibre interfaces and non-bonded regions were often observed. This could lead to reduction of properties, non-uniform stress distributions or reduced ability to transfer stress between consecutive elementary fibres. Using the circular cross-section assumption, the analysis of fibre CSA showed an overestimation of approximately 20 and 40 % for palm and coir technical fibres respectively. The measured average aspect ratio between the major axis and minor axis of technical fibres was 1.26 for palm and 1.28 and coir. The average CSA and aspect ratio of elementary fibres were 130 μm^2 and 1.34 for palm and 103 μm^2 and 1.37 for coir. The mechanical properties of palm and coir showed lower differences between diameter based and real CSA corrected values than expected from CSA measurements. This lower difference may be caused by the relation between the CSA distribution of tested samples and the variation of diameter based CSA versus real CSA trends according to different CSA ranges. The corrected average strengths of palm and coir were 116 and 149 MPa respectively. While tensile strength showed no significant

gauge length dependence, Young's modulus values were considerably dependent on test gauge length. Compliance corrections revealed similar Young's modulus for palm and coir technical fibres, 2.5 and 2.9 GPa respectively.

Two theoretical models were developed to fit to the observed Young's modulus dependence on fibre CSA. The models formulated the measureable modulus as a function of the dimensions of the technical fibre (defined as a multi-level structure) and the dimensions of the elementary along with the efficiency of the inter-level interface to transfer stress across consecutive levels. Both models generated almost equivalent predictions. In the case of palm, there was a good correlation between experimental observations and theoretical predictions. In the case of coir, due to higher variability of fibre properties and a lower CSA range of tested samples, the Young's modulus dependence on CSA was not as defined as for palm, which ultimately led to poorer correlations in terms of model fitting.

Acknowledgements

The authors gratefully acknowledge the financial support of SABIC Petrochemicals B.V. and the EPSRC Doctoral Training Grant scheme.

References

1. Eichhorn SJ, Baillie CA, Mwaikambo LY, Ansell MP, Dufrese A. Review of current international research into cellulosic fibers and composites. J Mater Sci 2001;36:2107–2131.
2. Raven PH, Evert RF, Eichhorn SE, Ray: Biology of plants. W.H. Freeman/Worth, New York 1999.
3. Bledzki AK, Gassan J. Composites reinforced with cellulose based fibres. Prog Polym Sci 1999;24:221–274.
4. Mussig J. ed: Industrial Applications of Natural Fibres. Wiley 2010.
5. Sathis review TP Sathishkumar TP, Navaneethakrishnan P, Shankar S, Rajasekar R, Rajini N. Characterization of natural fibre and composites–a review. J Reinf Plast Comp 2013;32:1457–1476.
6. Keya KN, Kona NA, Koly FA, Maraz KM, Islam MN, Khan RA. Natural fiber reinforced polymer composites: history, types, advantages, and applications. Mater. Eng. Res. 2019;1:69-87.
7. Cichocki FR, Thomason JL. Thermoelastic anisotropy of a natural fiber. Compos Sci Technol 2002;62:669–678.

8. Thomason JL. Why are natural fibres failing to deliver on composite performance? In Proceedings of the 17th International Conference on Composite Materials, Edinburgh, UK, 27–31 July 2009.
9. Thomason JL. Dependence of interfacial strength on the anisotropic fiber properties of jute reinforced composites. Polym Compos 2010;31:1525–1534.
10. Thomason JL, Yang L, Gentles F. Characterisation of the anisotropic thermoelastic properties of natural fibres for composite reinforcement. Fibers 2017;5(4):36.
11. Ntenga R, Béakou A, Atangana Atéba J, Ayina Ohandja L. Estimation of the elastic anisotropy of sisal fibres by an inverse method. J Mater Sci 2008;43:6206–6213.
12. Shah DU, Schubel PJ, Clifford MJ, Licence P. The tensile behavior of off-axis loaded plant fiber composites: An insight on the nonlinear stress–strain response. Polym Compos 2012;33:1494–1504.
13. Thomason JL, Carruthers J, Kelly J, Johnson G. Fibre cross-section determination and variability in sisal and flax and its effects on fibre characterisation. Compos Sci Technol 2011;71:1008–1015.
14. Baley C. Analysis of the flax fibres tensile behaviour and analysis of the tensile stiffness increase. Compos Part A Appl Sci Manuf 2002;33:939–948.
15. Tomczak F, Sydenstricker THD, Satyanarayana KG. Studies on lignocellulosic fibers of Brazil. Part II: Properties of Brazilian coconut fibers. Compos Part A Appl Sci Manuf 2007;38:1710–172.
16. Bodros E, Baley C . Study of the tensile properties of stinging nettle fibres. Mater Lett 2008;62:2143-2145.
17. Lamy B, Baley C. Stiffness prediction of flax fibers-epoxy composite materials. J Mater Sci Lett 2000;19:979-980.
18. Biagiotti J, Fiori S, Torre L, López-Manchado MA, Kenny J.M. Mechanical properties of polypropylene matrix composites reinforced with natural fibers. Polym Compos 2004;25:26–36.
19. Peponi L, Biagiotti J, Torre L, Kenny JM, Mondragon I. Statistical analysis of the mechanical properties of natural fibers and their composite materials. Polym Compos 2008;29(3):313-320.
20. De Rosa IM, Kenny J, Puglia D, Santulli C, Sarasini F. Morphological, thermal and mechanical characterization of okra fibre as reinforcement in composites. Compos Sci Technol 2010;70:116–122.
21. Griffith AA. The phenomena of rupture and flow in solids. Philos Trans R Soc London Ser.A, 1921;221:163–198.

22. Thomason JL, Carruthers J. Natural fibre cross sectional area, its variability and effects on the determination of fibre properties. J Biobased Mater Bioenergy 2012;6(4):424-430.
23. Deshpande AP, Bhaskar Rao M, Lakshmana Rao C. Extraction of bamboo fibers and their use as reinforcement in polymeric composites. J Appl Polym Sci 2000;76:83–92.
24. Williams GI, Wool RP. Composites from natural fibers. Appl Compos Mater 2000;7:421–432.
25. Juntaro J, Pommet M, Kalinka G, Mantalaris A, Shaffer MSP, Bismarck A. Creating hierarchical structures in composites by attaching bacterial cellulose to sisal fibers. Adv Mater 2008;20:3122-3126.
26. Rong MZ, Zhi M, Qiu M, Liu Y, Cheng G, Min H. The effect of fiber treatment on the properties of unidirectional sisal-reinforced epoxy composites. Compos Sci Technol 2001;60:1437-1447.
27. Martinschitz KJ, Boesecke P, Garvey CJ, Gindl W, Keckes J. Changes in microfibril angle in deformed dry coir fibers studied by in-situ synchrotron X-ray diffraction. J Mater Sci 2008;43:350–356.
28. Gassan J, Chate A, Bledzki AK. Calculation of elastic properties of natural fibers. J Mater Sci 2001;6:3715–3720.
29. Sreekala MS, Kumaran MG, Thomas S. Oil palm fibers: Morphology, chemical composition, surface modification, and mechanical properties. J Appl Polym Sci 1997;66:821–835.
30. Kulkarni AG, Satyanarayana KG, Sukumaran K, Rohatgi PK. Mechanical behaviour of coir fibres under tensile load. J Mater Sci 1981;16:905–914.
31. Keckes J, Burgert I, Frühmann K, Müller M, Kölln K, Hamilton M, Burghammer M, Roth SV, Stanzl S, Fratzl P. Cell-wall recovery after irreversible deformation of wood. Nat Mater 2003:2:810–814.
32. Spatz H, Köhler L, Niklas KJ. Mechanical behaviour of plant tissues: composite materials or structures? J Exp Biol 1999;202:3269–3272.
33. Defoirdt N, Biswas S, De Vriese L, Tran LQN, Acker JV, Ahsan Q, Gorbatikh L, Vuure AV, Verpoest I. Assessment of the tensile properties of coir, bamboo and jute fibre. Compos Part A Appl Sci Manuf 2010;41:588–595.
34. Joffe R, Andersons J, Wallström L. Strength and adhesion characteristics of elementary flax fibres with different surface treatment. Compos Part A Appl Sci Manuf 2003;34:603–12.
35. Cui S, Kinloch IA, Young RJ, Noé L, Monthioux M. The effect of stress transfer within double-walled carbon nanotubes upon their ability to reinforce composites. Adv Mater 2009;21:3591–3595.

36. Zalamea L, Kim H, Pipes RB. Stress transfer in multi-walled carbon nanotubes. Compos Sci Technol 2007;67:3425–3433.
37. Ashby MF, Medalist RFM. The mechanical properties of cellular solids. Metall Mater Trans A 1983;14:1755–1769.
38. Gibson LJ, Ashby MF, Schajer GS, Robertson CI. The mechanics of two-dimensional cellular materials. Proc R Soc A Math Phys Eng Sci 1982;382:25–42.
39. Gibson LJ. Biomechanics of cellular solids. J Biomech 2005;38:377–399.
40. Fratzl P, Weinkamer R. Nature's hierarchical materials. Prog Mater Sci 2007;52:1263–1334.
41. Thomason JL, Rudeiros-Fernández JL. A review of the impact performance of natural fibre thermoplastic composites. Frontiers in Materials 2018;5:60.

Figure Captions

Figure 17. E_f/E_{fr} according to Equation 19 for variable number of levels (n) and interfacial stress transfer efficiency (η).

Figure 18. Circular natural fibre model.

Figure 19. Comparison of honeycomb (solid lines) and circular (open circles) model predictions for E_f/E_{fr} for different fibre sizes and internal interfacial stress transfer efficiency

Figure 20. Honeycomb model for inter-fibre properties variability.

Figure 21. Palm Young's modulus versus CSA. Experimental and fitted theoretical models.

Figure 22. Coir Young's modulus versus CSA. Experimental and fitted theoretical models.

Tables

	Technical Fibre CSA (μm^2)		Elementary Fibre CSA (μm^2)	
	Mean	95% Confidence limits	Mean	95% Confidence limits
Palm	109530	28342	129.7	6.3
Coir	38085	5668	103.3	7.1

Table 1. Average CSA of palm and coir technical and elementary fibres

Sample	Young's modulus [GPa]		Tensile strength [MPa]		Failure strain [%]	
	Mean	95% Confidence limits	Mean	95% Confidence limits	Mean	95% Confidence limits
Palm all	**2.4**	**0.2**	**116**	**10**	**39.1**	**8.9**
Palm 5 mm	1.7	0.3	125	19	65.3	21.0
Palm 10 mm	2.5	0.3	114	17	28.8	8.1
Palm 20 mm	2.8	0.3	109	15	21.5	4.5
Coir all	**2.4**	**0.2**	**149**	**12**	**38.1**	**3.0**
Coir 5 mm	1.9	0.3	169	21	49.9	4.6
Coir 10 mm	2.1	0.2	122	18	39.2	3.7
Coir 20 mm	3.2	0.3	156	22	24.9	2.3

Table 2. Palm and coir fibre tensile properties.

Gauge length (L_0)	Palm		Coir	
	E_f (GPa)	C_s (μm/N)	E_f (GPa)	C_s (μm/N)
5 mm	1.90	7.0	2.50	26.3
10 mm	2.65	5.5	2.85	23.3
20 mm	2.67	2.9	2.91	2.7

Table 3: Technical fibre modulus and compliance factor obtained at individual gauge lengths.

Sample	l [μm]	Honeycomb model			Circular model		
		E_{fr} [GPa]	η	R^2	E_{fr} [GPa]	η	R^2
Palm (5 mm)	6.9	5.04	0.67	0.82	4.73	0.65	0.81
Coir (5 mm)	6.2	2.93	0.85	0.15	2.90	0.83	0.16

Table 4. Theoretical fitting models results.

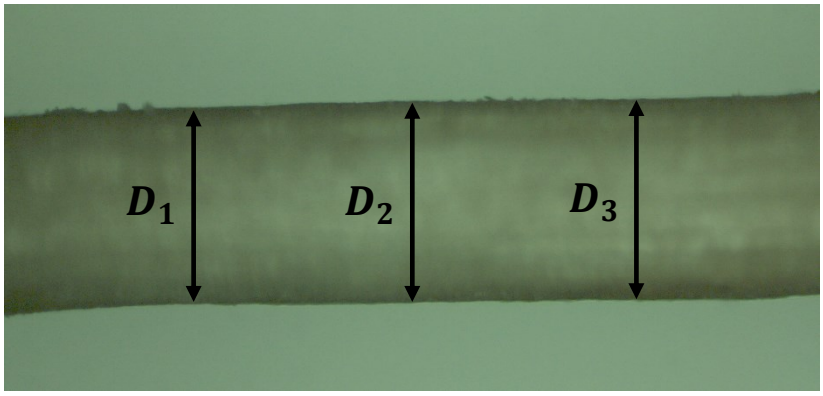

Figure 1. Diameter transverse observation for circular CSA calculation

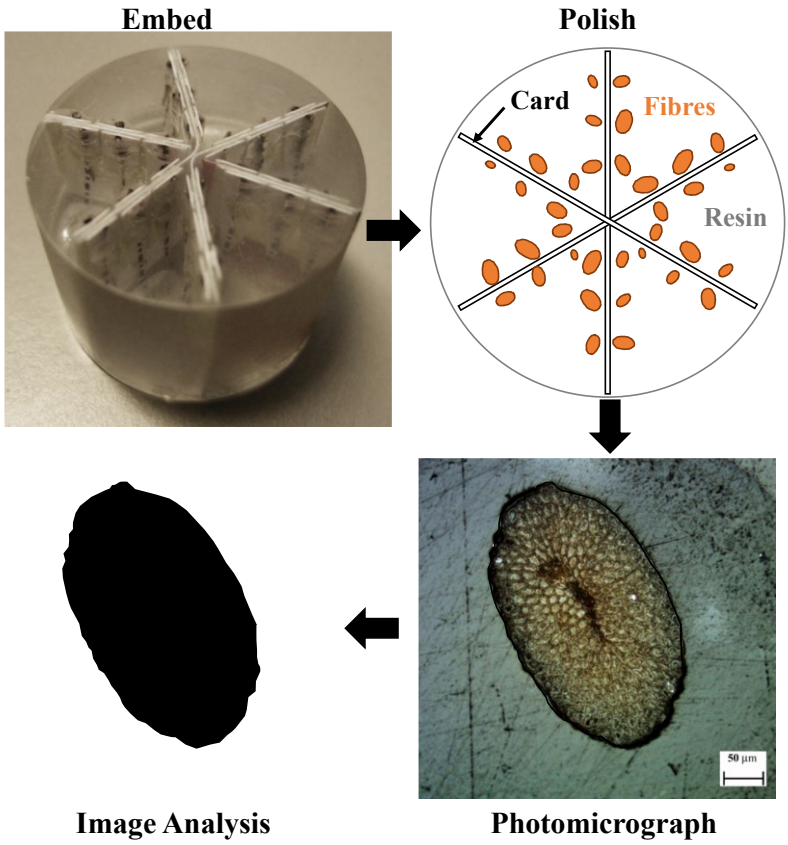

Figure 2. Process of determining the true CSA measurements of natural fibres

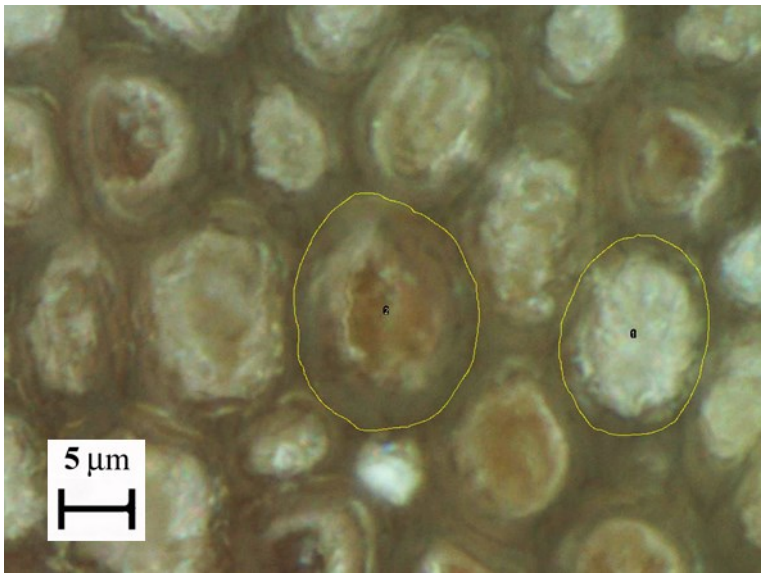

Figure 3. Detail of the CSA of palm fibre. Measurement of elementary fibres.

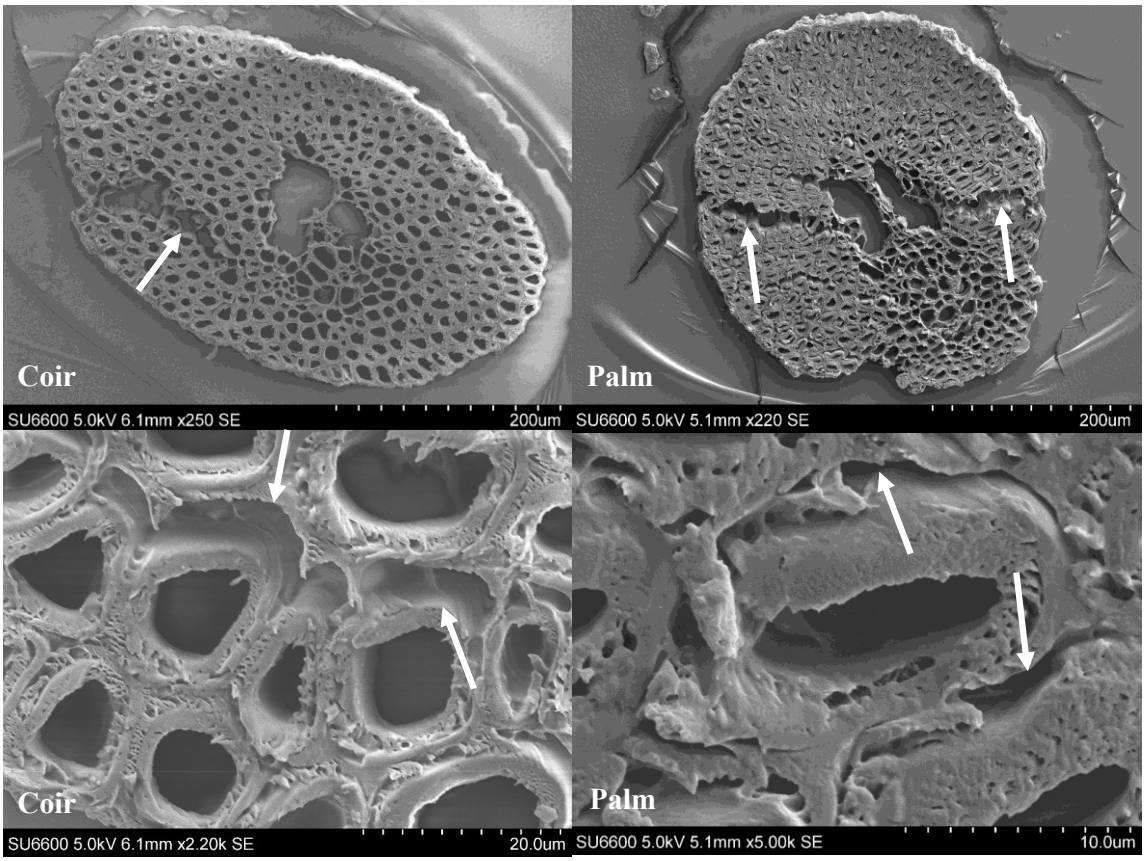

Figure 4. SEM micrographs of cryotome cut natural fibre sections

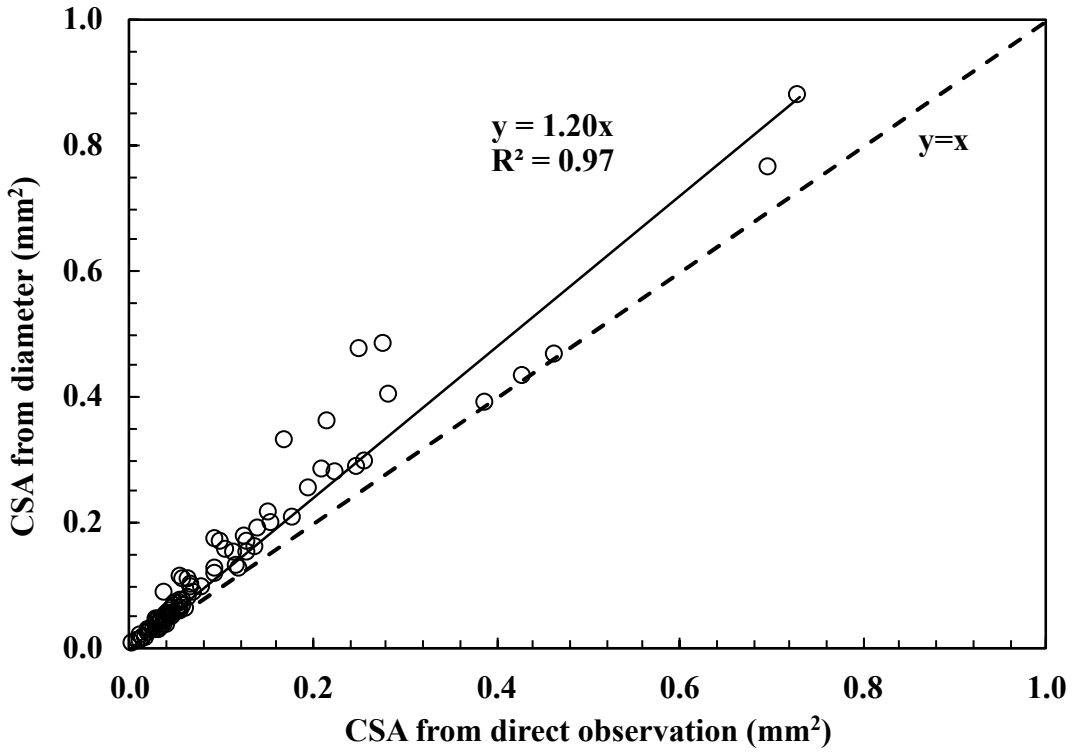

Figure 5. Palm fibre CSA - direct observation versus "diameter" method.

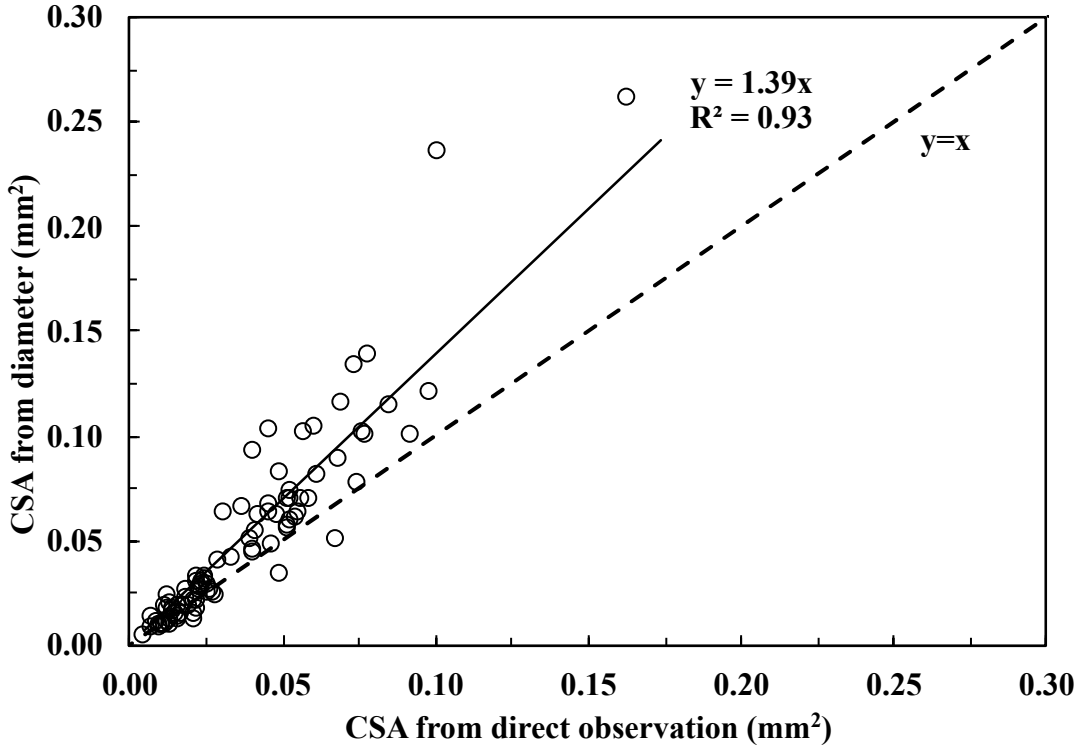

Figure 6. Coir fibre CSA - direct observation versus "diameter" method.

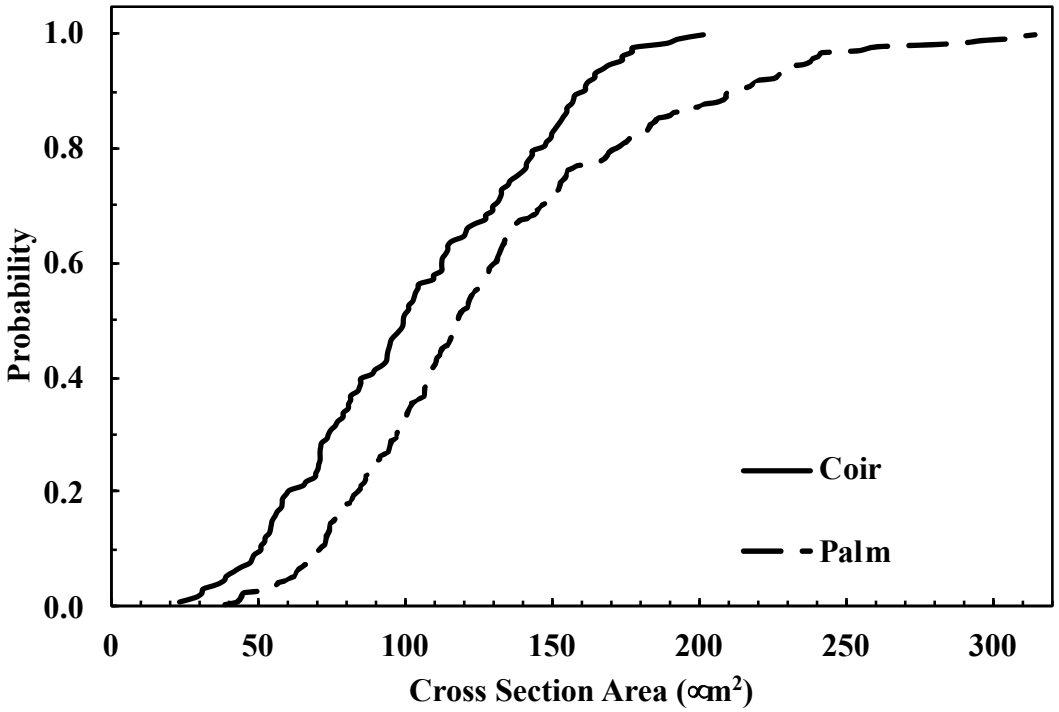

Figure 7. Elementary fibre CSA distribution.

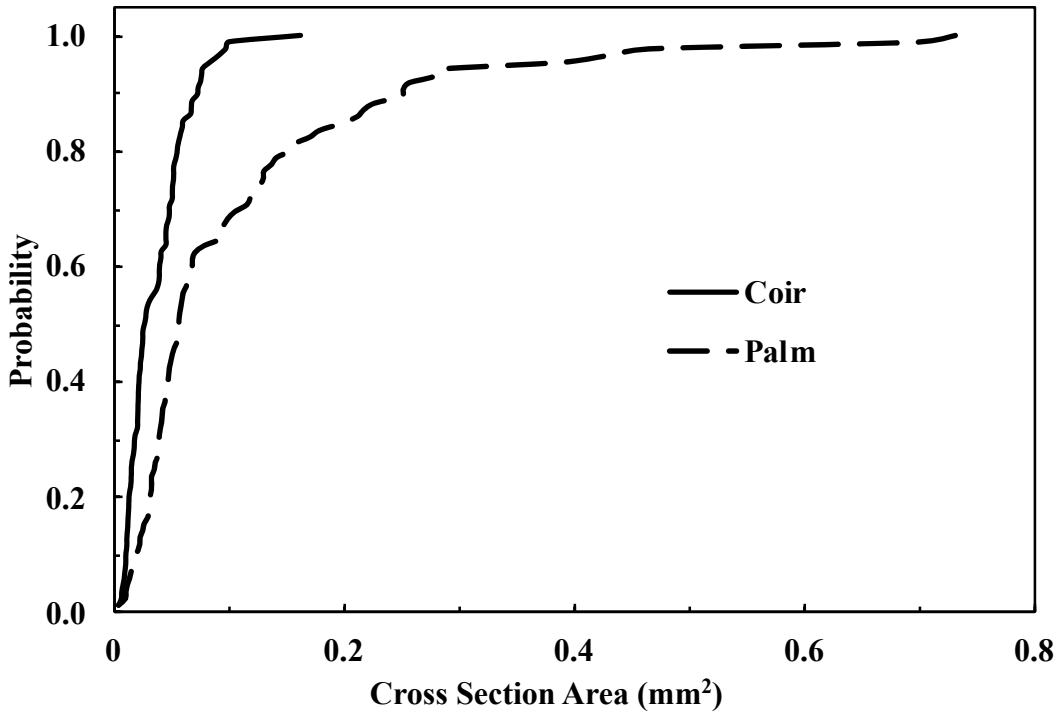

Figure 8. Technical fibre CSA distribution.

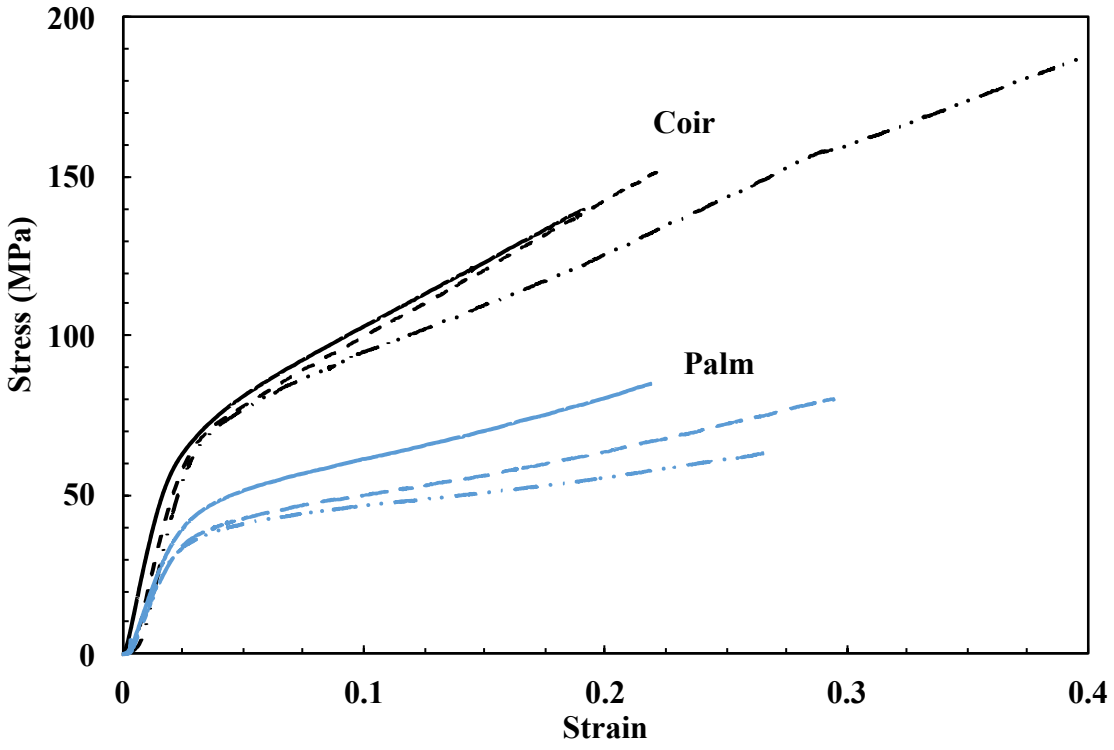

Figure 9. Typical coir and palm stress-strain curves at 20 mm gauge length.

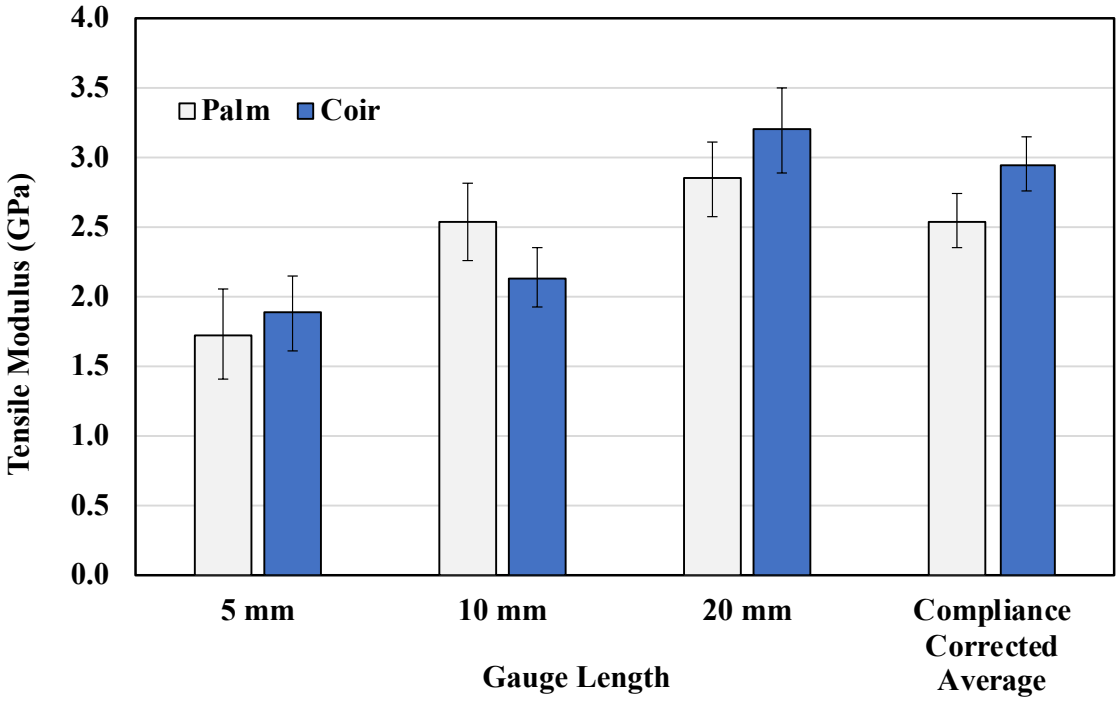

Figure 10. Young's modulus for three different gauge lengths and compliance corrected.

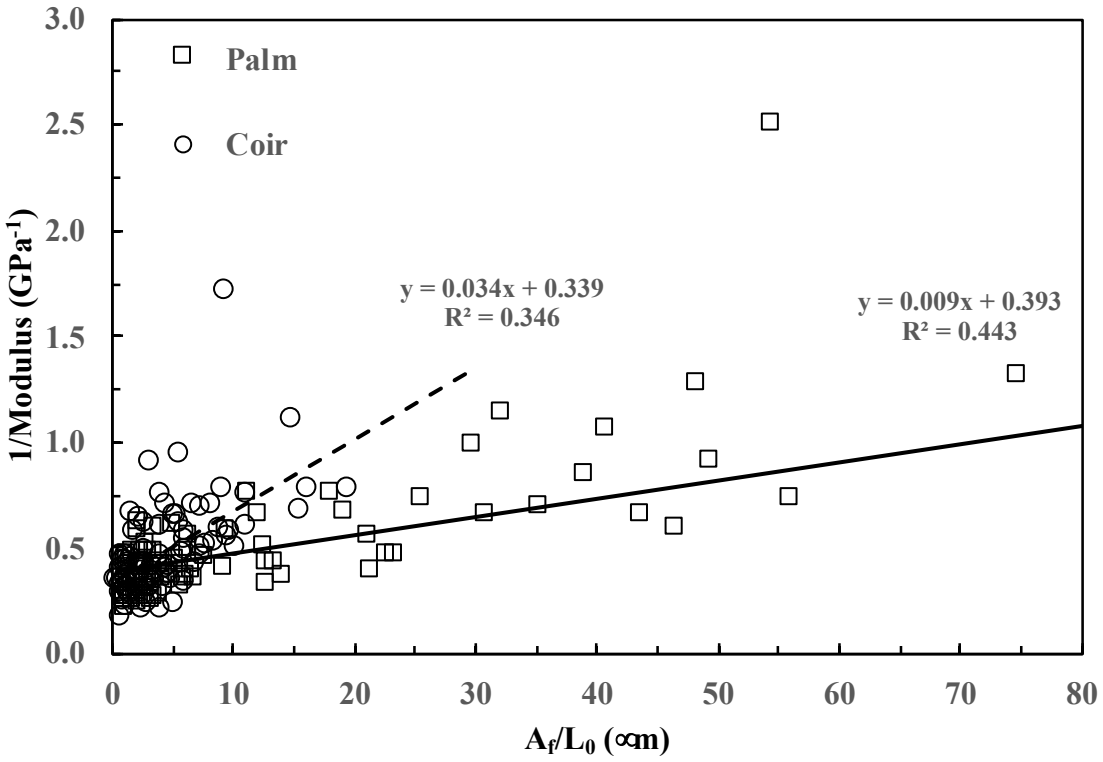

Figure 11. Compliance correction analysis for fibre modulus

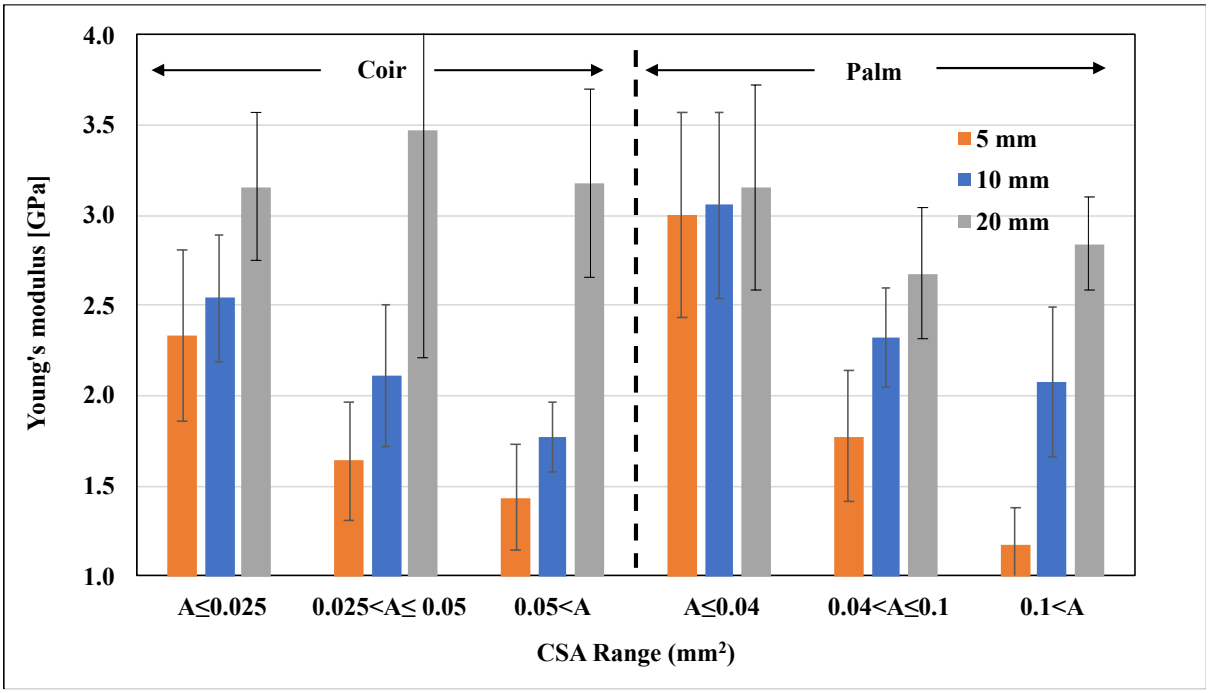

Figure 12. Coir and Palm fibre modulus for three different CSA ranges.

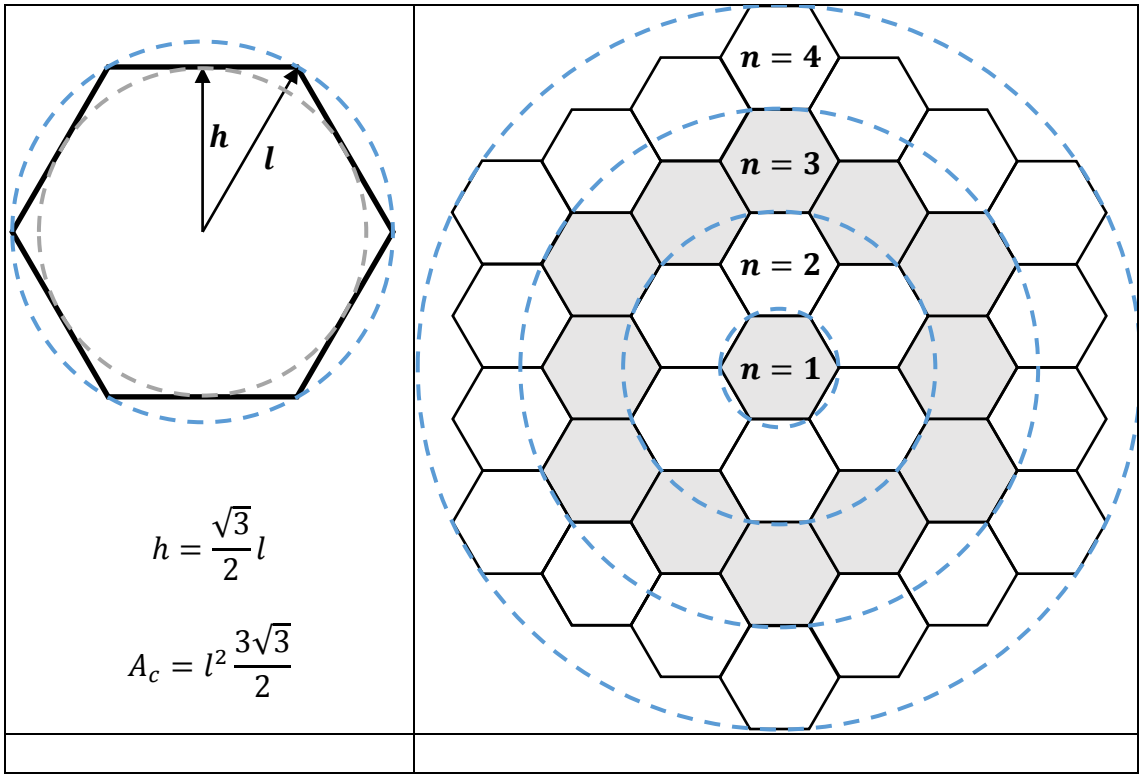

Figure 13. Natural fibre hexagonal cell model structure.

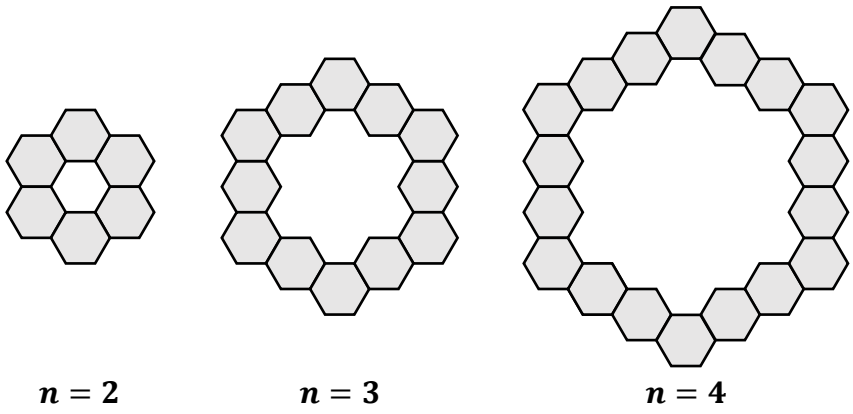

Figure 14. Equivalent hollow fibres.

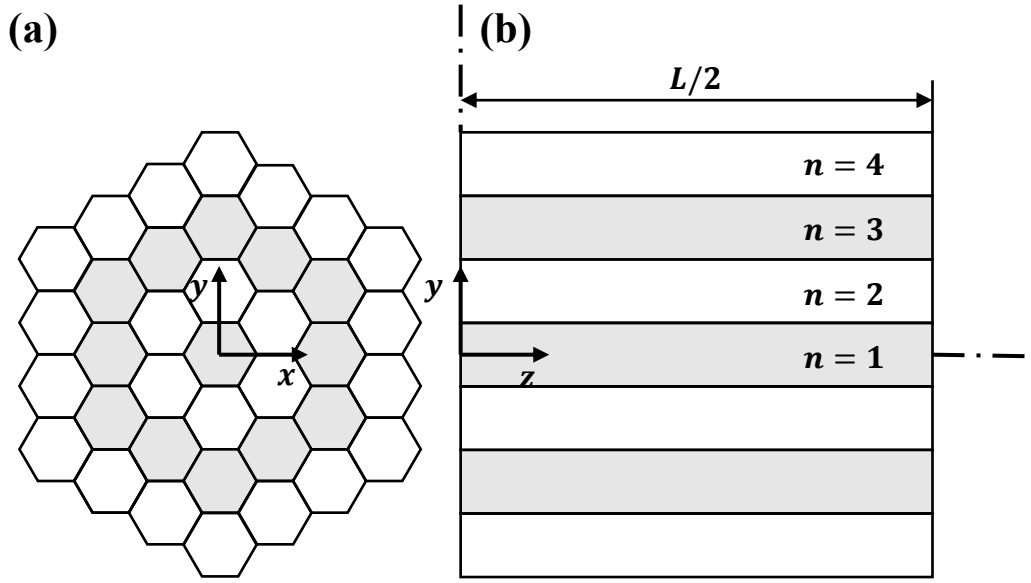

Figure 15. Natural fibre honeycomb model. (a) Cross section view of the model, where the origin xy is located in the centre of the central cell (i.e. $n = 1$) and the middle point of the fibre length L. (b) Longitudinal view of the model in the plane yz.

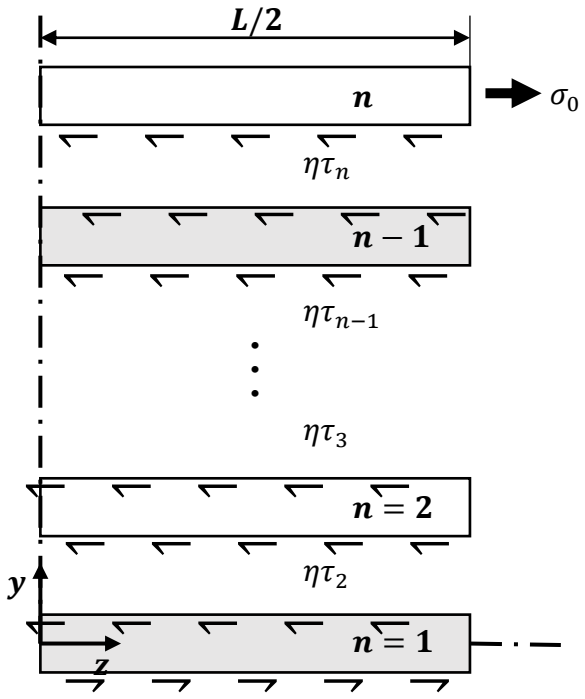

Figure 16. Stress transfer between levels. The fibre is made up by the n-levels.

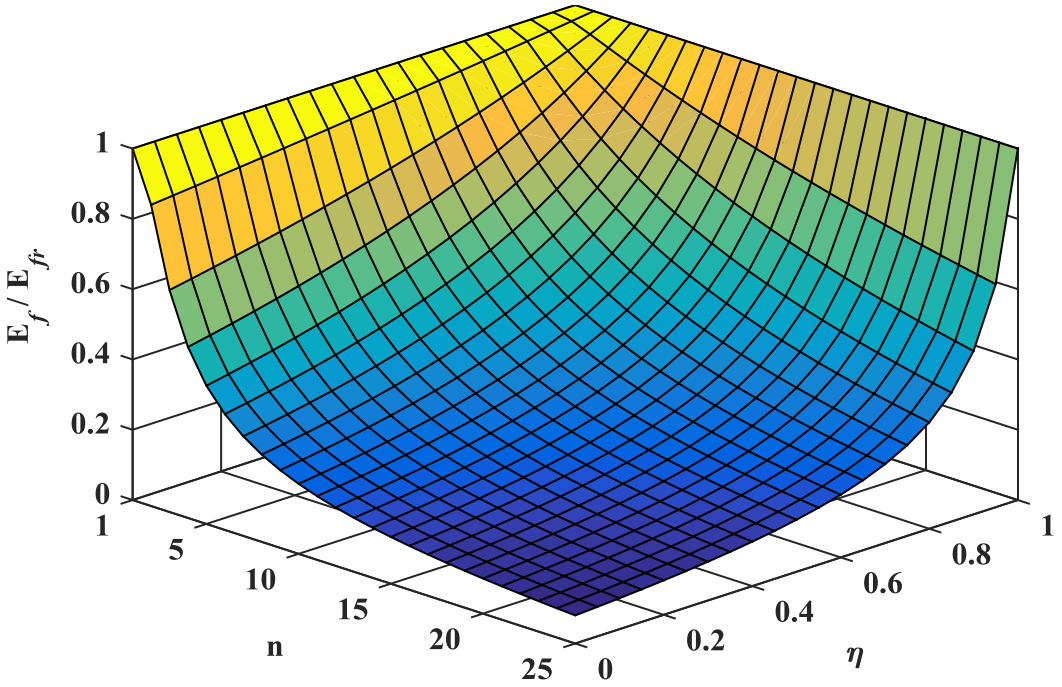

Figure 17. E_f/E_{fr} according to Equation 19 for variable number of levels (n) and interfacial stress transfer efficiency (η).

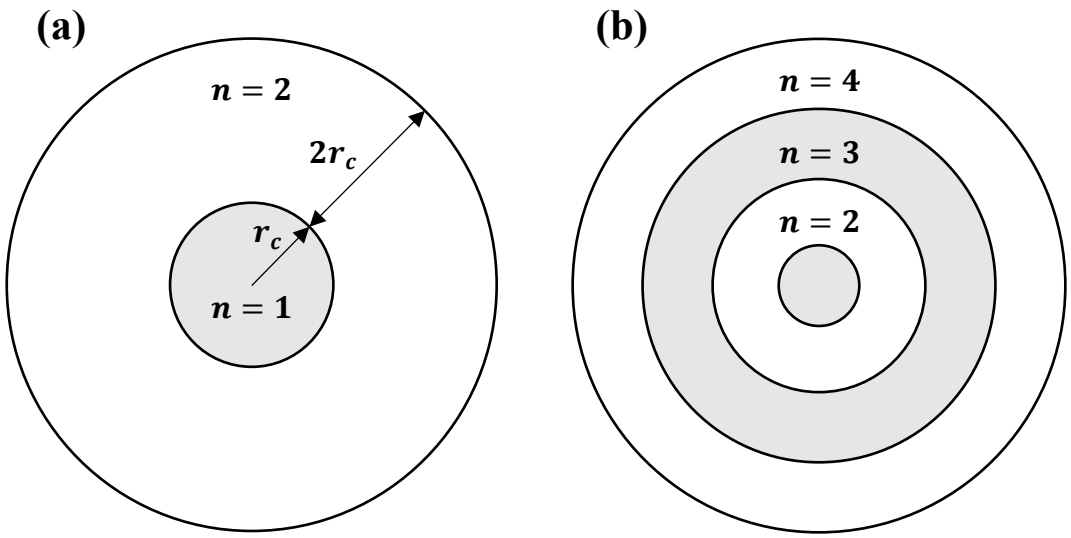

Figure 18. Circular natural fibre model.

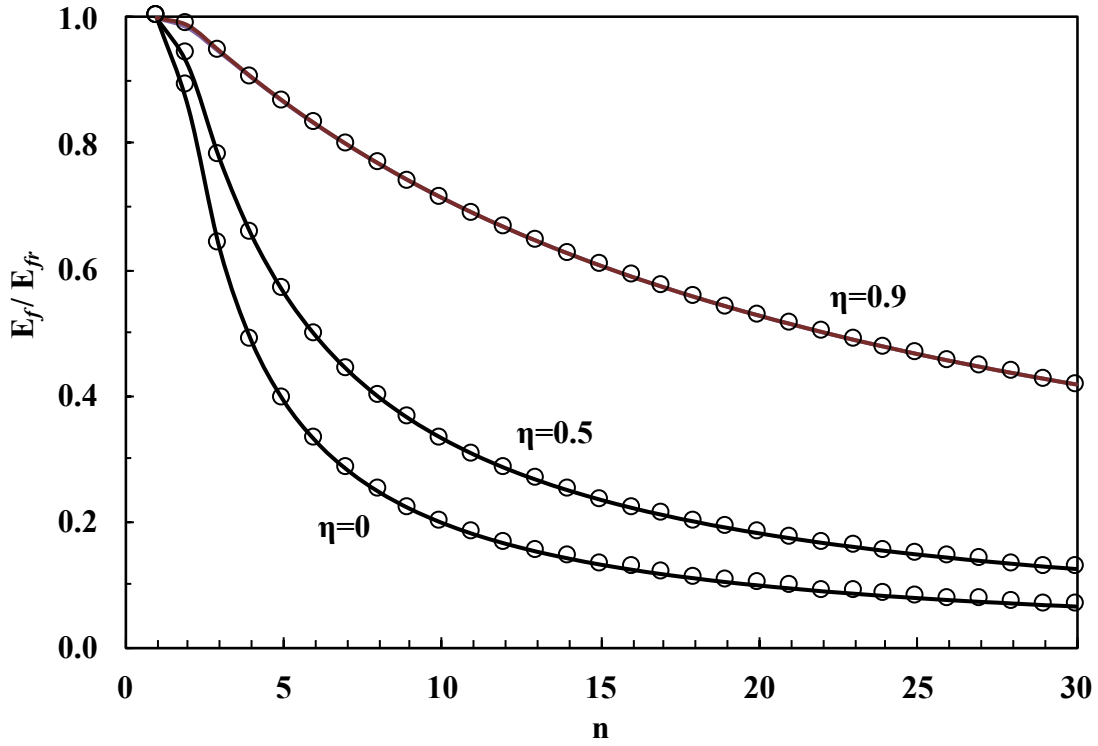

Figure 19. Comparison of honeycomb (solid lines) and circular (open circles) model predictions for E_f / E_{fr} for different fibre sizes and internal interfacial stress transfer efficiency

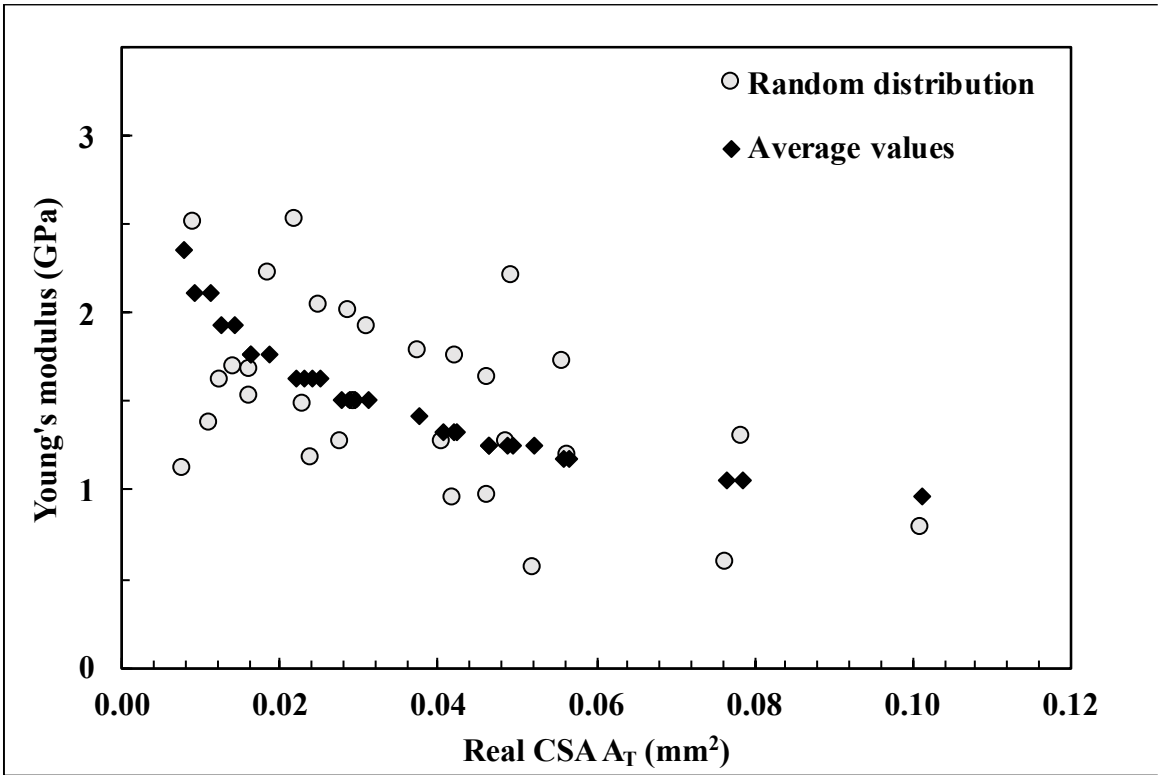

Figure 20. Honeycomb model for inter-fibre properties variability.

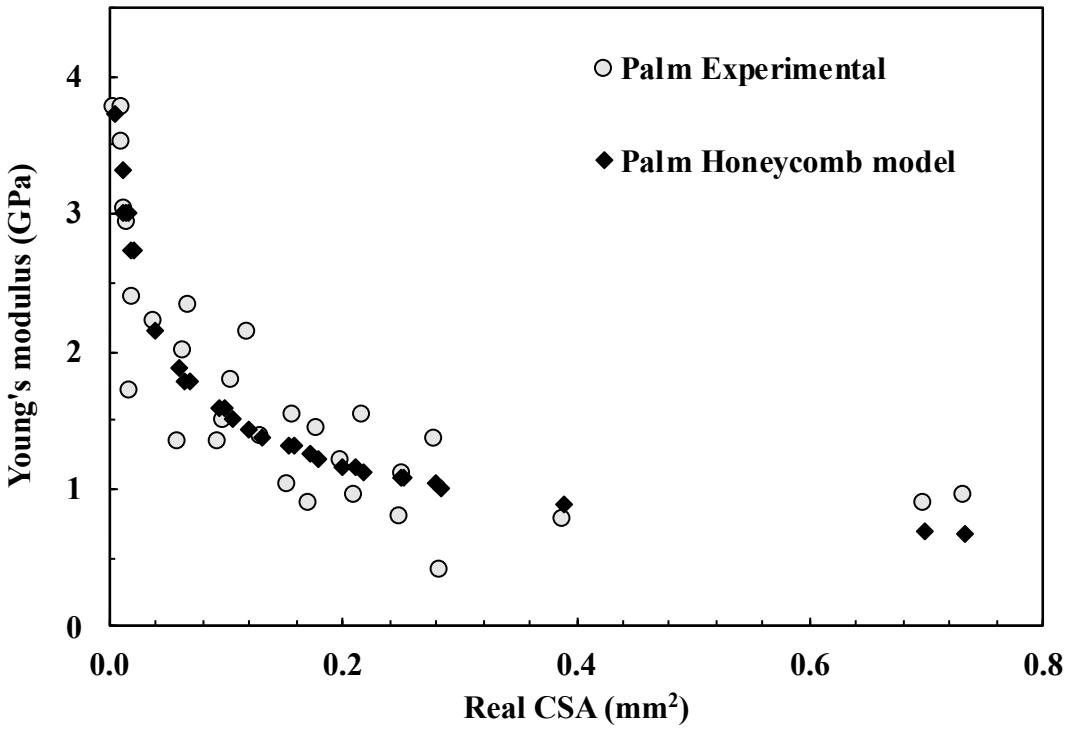

Figure 21. Palm Young's modulus versus CSA. Experimental and fitted theoretical models.

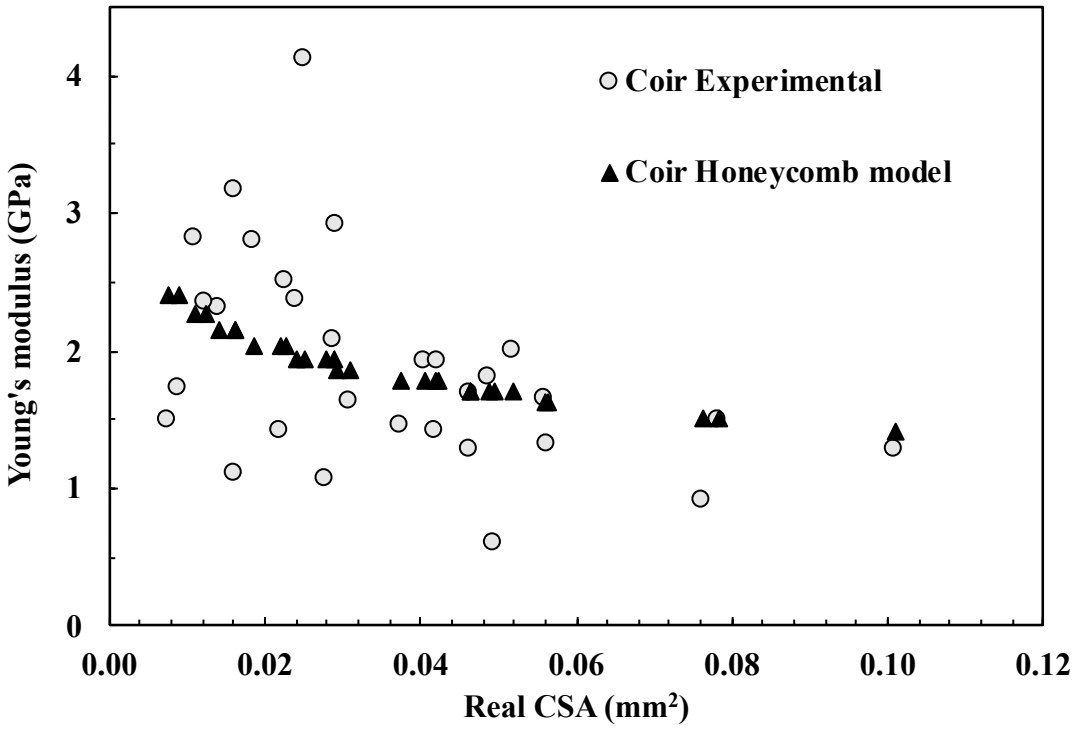

Figure 22. Coir Young's modulus versus CSA. Experimental and fitted theoretical models.